

PAPER • OPEN ACCESS

Surface plasmons on ordered and bi-continuous spongy nanoporous gold

To cite this article: Neha Sardana *et al* 2014 *New J. Phys.* **16** 063053

View the [article online](#) for updates and enhancements.

Related content

- [Radiation guiding with surface plasmon polaritons](#)
Zhanghua Han and Sergey I Bozhevolnyi
- [Enhancement of the magneto-optical Kerr effect signal using bilayer metallic structures consisting of Co/noble metal](#)
Thanachai Dasri and Artit Chingsungnoen
- [Topical Review](#)
Emmanuel Fort and Samuel Grésillon

Recent citations

- [James A. Dolan](#)
- [Ultrafast surface plasmon-polariton interference and switching in multiple crossing dielectric waveguides](#)
Tobias Birr *et al*
- [Gyroid Optical Metamaterials: Calculating the Effective Permittivity of Multidomain Samples](#)
James A. Dolan *et al*



IOP | ebooks™

Bringing you innovative digital publishing with leading voices to create your essential collection of books in STEM research.

Start exploring the collection - download the first chapter of every title for free.

Surface plasmons on ordered and bi-continuous spongy nanoporous gold

Neha Sardana^{1,2}, Tobias Birr³, Sven Schlenker⁴, Carsten Reinhardt³ and Jörg Schilling¹

¹ Centre for Innovation Competence SiLi-nano, Martin Luther University of Halle-Wittenberg, Karl-Freiherr-von-Fritsch-Str. 3, D-06120 Halle (Saale), Germany

² International Max Planck Research School for Science and Technology of Nanostructures, Weinberg 2, D-06120 Halle (Saale), Germany

³ Laser Zentrum Hannover e.V., Hollerithallee 8, D-30419 Hannover, Germany

⁴ Interdisciplinary Center of Material Science, Martin Luther University of Halle-Wittenberg, Heinrich-Damerow-Str. 4, D-06120 Halle (Saale), Germany

E-mail: neha.sardana@physik.uni-halle.de and joerg.schilling@physik.uni-halle.de

Received 25 November 2013, revised 28 April 2014

Accepted for publication 21 May 2014

Published 24 June 2014

New Journal of Physics **16** (2014) 063053

[doi:10.1088/1367-2630/16/6/063053](https://doi.org/10.1088/1367-2630/16/6/063053)

Abstract

The dispersion relation and propagation of surface plasmons polaritons (SPPs) on nanoporous gold films is experimentally investigated and an increasing red shift of the SPPs is observed with rising porosity. This is caused by a less negative effective dielectric constant of the nanoporous metal films and is predicted by classical Bruggeman or specific two dimensional Maxwell-Garnett effective medium models. The dispersion relation data is supported with leakage radiation microscopy enabling the determination of the propagation length and losses of surface plasmons on these nanoporous films. These results demonstrate how the control of the nanoporosity of metal layers leads to designer plasmons in the visible and near infrared allowing the tuning of the SPP dispersion to match the requirements of certain applications.

Keywords: surface plasmons, optical properties, nanoporous films



Content from this work may be used under the terms of the [Creative Commons Attribution 3.0 licence](https://creativecommons.org/licenses/by/3.0/). Any further distribution of this work must maintain attribution to the author(s) and the title of the work, journal citation and DOI.

1. Introduction

Silver and gold have dominated the field of plasmonics for a long time as materials of choice, due to their high conductivity and comparatively low losses. However, recently the search for other metallic materials with less negative values of the permittivity but comparable low losses has emerged due to a strong interest in epsilon-near-zero metamaterials as they allow impedance matching of plasmonic components and scattering suppression [1, 2]. Due to these efforts, new classes of organic and inorganic compounds have entered the field of plasmonics [3, 4]. On the other hand especially the morphology of gold has been tailored widely on the nanoscale, creating nanopores, voids, inclusions, or specific surface topographies. The optical response of this nanoporous or structured gold, measured as transmittance or absorption, show large variations compared to the bulk. Its versatility opened up a large area of applications in sensing, non-linear optics, and imaging [5], to name just a few. Several theories and simulations [6–9] have been successfully implemented to describe the plasmonic behaviour of nanoporous gold.

However up to now mainly localized surface plasmons on metal nanoparticles or coupled surface plasmons on closely positioned particles and particle chains were investigated. The formation of collective designer surface plasmons [10–12] on metal surfaces, which are deliberately structured on the sub-wavelength scale, was only investigated experimentally in the microwave region. On the other hand the possibility to gain control over the surface plasmon-polariton (SPP) dispersion relation by controlling the porosity of metal films has the potential to lead to tailor-made SPPs for specific applications, where the involved dielectric materials are given and the SPP-frequencies have to be adjusted. Therefore, in this paper we present studies on measurements of the SPP dispersion and SPP propagation properties on the surface of nanoporous gold samples. Random bi-continuous spongy nanoporous gold films as well as hexagonally self-ordered nanoporous gold films are fabricated and investigated. The samples are experimentally characterized using two different methods: spectrally resolved reflection measurements in Kretschmann configuration and leakage radiation microscopy (LRM). We investigate the effect of the porous nanostructure on the SPP propagation, their dispersion relation, and its effect on SPP-light scattering [13–16]. LRM is demonstrated as a particularly powerful quantitative technique, allowing both the imaging of the real sample and back focal plane, also referred to as the Fourier plane (FP). This method provides a convenient direct determination of SPP propagation length and the real part of the SPP wave vector, from which the SPP dispersion is easily obtained.

2. Experimental details

2.1. Sample fabrication and structural investigation

Two different types of nanoporous gold films have been prepared by the following two methods: first, the bi-continuous spongy nanoporous gold films have been realized by dealloying of 12 carat white gold leaves (50 wt.% Au and 50 wt.% Ag) for 60 min in conc. HNO_3 . Second, the hexagonally ordered gold films have been prepared by thermally evaporating gold on porous alumina templates (Smart Membranes GmbH) with hexagonally ordered pores of 30 nm and 55 nm diameter. After gold deposition the alumina templates are

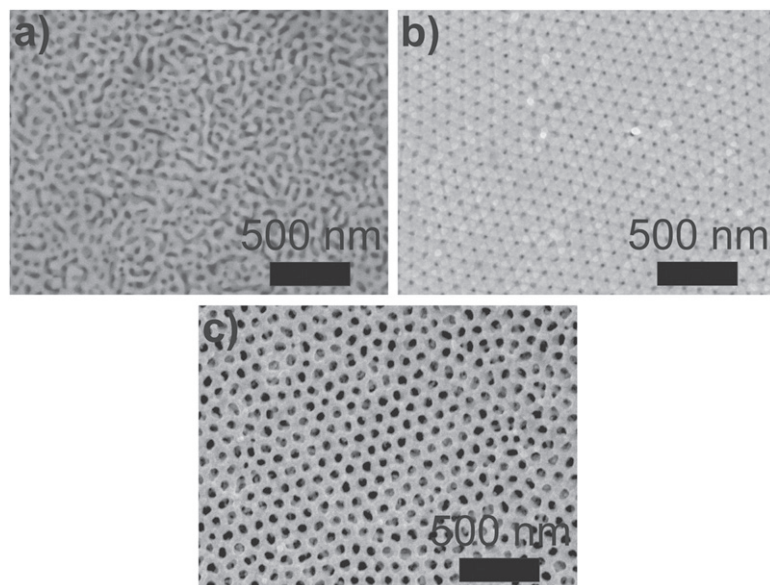


Figure 1. SEM images of porous gold samples under investigation. (a) 12 carat gold dealloyed in HNO_3 for 60 min. Hexaporous Au film formed from Au deposition on (b) 30 nm Alumina template (c) 55 nm Alumina template etched in 50 wt% KOH. All structure sizes are considerably smaller than the wavelength of visible light.

dissolved in 50 wt.% KOH solution. These samples are further referred to as hexaporous gold films.

Subsequently, all nanoporous gold films have been floated on water in order to remove residual amounts of acid or alkali. Finally, the films have been placed on a glass slide (*BK7*) and the water has been allowed to evaporate at room temperature.

For structural characterization of the resulting nanoporous gold films a JEOL scanning electron microscope (SEM) has been used. The respective images are shown in figure 1. X-ray spectroscopic (EDS) measurements confirm a 100% pure porous Au-film without any remains of silver for the dealloyed sample [17] and no residual alumina for the hexaporous gold films. The film thickness of the individual samples has been measured by x-ray reflectometry to approx. 50 nm. For reference and comparisons a 50 nm thick non-porous ‘bulk’ gold film is considered, which has also been deposited on a glass slide by thermal evaporation.

2.2. Experimental measurement of optical properties

The spectrally resolved optical properties of the nanoporous gold films have been determined by surface plasmon resonance (SPR) measurements. SPP on the nanoporous film surface are excited using prism coupling in Kretschmann configuration [13, 17]. In this setup, the glass slide carrying the metal film has been attached to the base of a right angled prism (*BK7* glass, $\epsilon = 2.25$) with a drop of *L4085AGAR* immersion oil ($\epsilon = 2.3$, Plano labs, Germany). A beam of white light from a halogen lamp (200 W) is linearly polarized using a birefringent crystal polarizer and is incident on one of the prism’s side facets. The light which is reflected from the sample at the base of the prism exits via the opposite prism side facet and is picked up by a fiber bundle of a grating spectrometer. By rotating the prism and the detecting fiber bundle this setup allows the measurement of spectrally resolved reflection measurements for fixed incidence

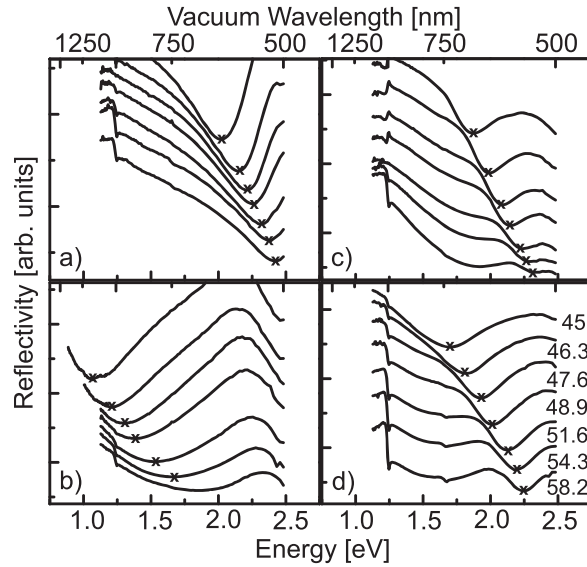


Figure 2. Angular resolved reflectivity spectra in Kretschmann configuration. The plotted curves represent the ratio of p-polarized/s-polarized reflection for (a) bulk gold film [17], (b) nanoporous gold film [17], (c) 30 nm hexaporous gold and (d) 55 nm hexaporous gold. The values of the angles of incidence in the glass are the same for all curves. A dip in reflection occurs, which shifts to shorter wavelengths with increasing angle of incidence (marked by the crosses). This indicates the resonant excitation of propagating surface plasmons.

angles in the range of $45^\circ \leq \theta \leq 68^\circ$ for s- and p-polarized light. The excitation of a surface plasmon is indicated by a characteristic dip in reflectivity for p-polarized light, which shifts to shorter wavelengths with increasing angle of incidence. To cancel out the common negative slope in the reflectivity of s- and p-polarized spectra due to the onset of interband absorption, the ratio of p-/s-polarized spectra is taken and is shown in figure 2. This allows a more accurate determination of the dip-position of the p-polarized spectra.

From the position of the minima in the reflection spectra the real part of the SPP wave vector (k_x)_r can be determined easily. Additionally, LRM of the propagating SPPs [14, 18–20] is used as a tool to directly determine the real part of the SPP wave vector as well as the imaginary part (k_x)_i by measuring the SPP propagation length. The principle is demonstrated for an excitation wavelength of $\lambda = 780$ nm. The SPPs are launched by focussing the laser radiation onto a slit in the bulk/nanoporous gold layer which has been fabricated by focussed ion beam (FIB) milling.

SPPs propagating along the air/gold interface couple to light modes in the glass substrate [21, 22]. This leakage radiation is imaged through an oil immersion objective (100X, Numerical Aperture (NA) = 1.4, Zeiss) onto a CCD camera (ABS Jena). A scheme of the setup can be found in the appendix. The setup allows to switch between imaging the back focal plane and the real image plane (IP) onto the CCD. The back focal plane corresponds to the FP of the image which allows access to the angle at which the light is emitted and the wave vectors involved [23]. Figure 3 shows all the IP and FP images and their respective intensity profiles for the investigated samples. A beam block (seen as dark central region in the FP images) is used in the

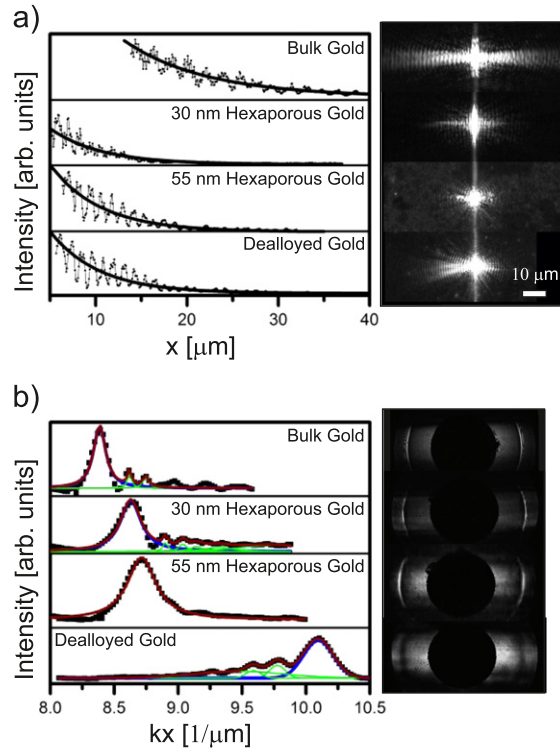


Figure 3. Leakage radiation microscopy. (a) real plane image and its data (symbols) fitted with exponential decay profiles (solid line). (b) Fourier plane image and its corresponding intensity profile (symbol) fit with a system of Lorentzian peaks (solid lines).

back focal plane of all images to block the strong directly transmitted laser light. The diagrams in 3(a) represent the intensity traces at horizontal cross-sections of the IP, while the diagrams in 3(b) are the cross-sections in the FP. The sharp crescents far away from the FP-centre are the signatures of the SPP leakage radiation. They correspond to the large peaks in the adjacent diagrams.

3. Results and discussion

3.1. Dispersion relation from SPR measurements

Comparing the spectral position of the dips in the angular resolved reflection spectra of figure 2 one already observes the shift of the excited surface plasmons to lower energies (red shift) when a porosity is introduced in the metal layer. For instance, at an incidence angle of 45° a clear red shift of up to 0.94 eV for the dealloyed gold sample with respect to bulk gold sample is observed. To obtain an overview of the changes of the surface plasmon frequencies and its associated wave vectors the SPP dispersion can be plotted using the spectral positions of the dips.

Applying [13]: $k_x = \sqrt{\epsilon_g} \frac{\omega}{c} \sin \theta$ the real part $(k_x)_r$ of the SPP wave vector can be determined from the frequency ω and the angle θ at which the dip in reflection occurs in figure 2. The resulting experimental data points for k_x and ω are marked as symbols in figure 4. They represent the experimentally mapped dispersion relation of the SPPs on all four samples

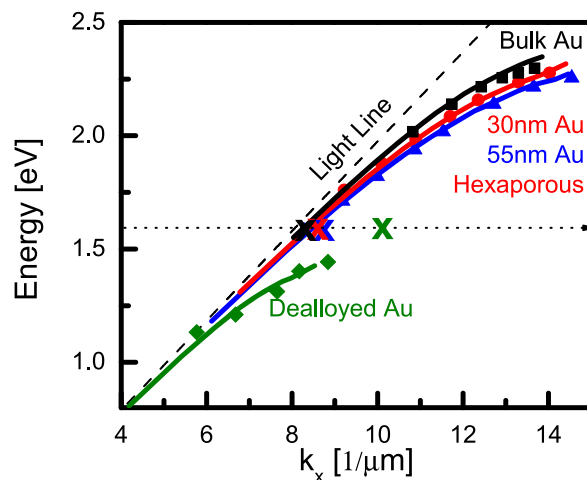


Figure 4. Dispersion relation of propagating surface plasmons at the bulk gold film (black), spongy dealloyed nanoporous gold (green), the hexaporous gold film with 30 nm pore diameter (red) and 55 nm pore diameter (blue). The experimental data is shown as symbols and solid lines are the effective medium model fittings. The crosses at 780 nm = 1.59 eV correspond to wave vectors obtained from the FP analysis.

and confirm the already observed red shift of the SPP dispersion relation for the nanoporous samples. This shift is caused by the increase of the effective dielectric constant (ϵ_{eff}) of the nanoporous gold i.e. ϵ_{eff} has a less negative value since the nanoporous gold films act like ‘diluted’ metals [13, 17].

This experimental shift in the dispersion relation is compared with theoretical calculations using effective dielectric constants for the nanoporous gold films. As the dealloyed spongy gold is a three dimensional random, interlinked structured, it can be well fitted with the Bruggeman effective medium theory [24]. However, the hexaporous samples consist of an array of vertical aligned pores (which are isolated from each other) in a gold matrix. For this optically anisotropic uniaxial structure we apply 2D Maxwell-Garnett theory [9, 25] with the following two principal effective dielectric constants: $\epsilon_{\parallel} = f\epsilon_a + (1 - f)\epsilon_m$ and $\epsilon_{\perp} = \frac{(1+f)\epsilon_a + (1-f)\epsilon_m}{(1-f)\epsilon_a + (1+f)\epsilon_m}$ where, ϵ_a , ϵ_m are the dielectric constants for air rods and metal matrix respectively. To use these formulas, we need to input the air fraction f for each sample. The fill fraction for dealloyed gold is determined using the volume loss of the film [17] after dealloying, whereas the porosity of the hexaporous samples is directly calculated from the SEM images using the ImageJ software. Following these procedures we determined $f = 0.2, 0.3$ and 0.5 for hexaporous 30 nm and 55 nm and dealloyed gold respectively. Using the optical data of gold from Johnson and Christie the SPP-dispersion curves for nanoporous gold could finally be calculated. A comparison between the experimentally determined dispersion data and the theoretically derived dispersion curves in figure 4 shows a good agreement.

3.2. LRM

Using the results from LRM the propagation length of the SPP can be determined in two different ways: either by fitting an exponential decay to the SPP-intensity trail in the real IP, or by evaluating the width of the crescents in the FP.

Fitting an exponential decay to each of the intensity profiles in figure 3(a) yields $L_{\text{spp}} = 9.0 \mu\text{m}$, $5.6 \mu\text{m}$, $3.7 \mu\text{m}$ and $4.5 \mu\text{m}$ for bulk gold, 30 nm, 55 nm hexaporous gold, and dealloyed gold, respectively. The faster decay of the SPPs at the nanoporous gold surfaces can be mainly assigned to increased radiative scattering losses due to surface roughness. Furthermore, the electronic oscillatory motion might already be damped by increased surface scattering of the electrons within the thin gold veins increasing the ohmic losses of the nanoporous material.

When one closely looks at the real images in figure 3(a) one can observe periodic intensity oscillations appearing on top of the exponential decay. These oscillations are caused by the interference of the SPP leakage radiation and the homogeneously scattered light which is collected by the NA of the objective [16]. For the microscope objective with a NA of 1.4, we calculated $\Lambda_l = \frac{2\pi}{NAk_0 - k_{\text{spp}}} = 2.069 \mu\text{m}$ and $\Lambda_s = \frac{2\pi}{NAk_0 + k_{\text{spp}}} = 0.3219 \mu\text{m}$ as possible oscillation periods. From figure 3(a) one clearly observes Λ_l , while Λ_s can be observed only in a magnified view (found in the appendix). Comparing these oscillation periods with the experimental values of $2.01 \mu\text{m}$ and $0.33 \mu\text{m}$ for bulk gold shows a good agreement which confirms the interference effects as suggested in [16].

As mentioned before, the leakage radiation of the SPP forms crescents in the FP. They are positioned on a circle with radius $(k_x)_r$ and their intensity profile can be fitted by a Lorentzian curve [13, 14] $I = \frac{\text{const.}}{(K_x - (k_x)_r)^2 + (k_x)_i^2}$. The imaginary part of the surface plasmon wave vector $((k_x)_i)$ determines the full width at half maximum of the Lorentzian $\delta(k_x)_r = 2(k_x)_i$. With $L_{\text{spp}} = 1/2(k_x)_i$ one therefore obtains directly $L_{\text{spp}} = 1/\delta(k_x)_r$.

Besides the main Lorentzian peak of the crescent several smaller peaks are also visible in the intensity profile of the FP. They are supposed to be artefacts of the measurement but their origin is not quite clear yet. However, to obtain an accurate fit of the major peak the overlap with the smaller peaks have been taken into account. Therefore multiple Lorentzian's were fitted to all the peaks resulting in a faithful representation of the experimental profile. From the full width at half maxima we obtained $L_{\text{SPP}} = 8.8 \mu\text{m}$, $5.2 \mu\text{m}$, $3.5 \mu\text{m}$ and $4.4 \mu\text{m}$ for bulk gold, 30 nm, 55 nm hexaporous gold, and dealloyed gold, respectively. When these values are compared with the results determined from the exponential decays in the IP a reasonable correspondance can be observed as it is expected from the theoretical model. The slight discrepancy which is still present might be attributed to the background scattered light. The radiative losses due to scattering on the surface roughness result in a considerable radiation background which leads to an overall increase in the observed radiation in the IP. This can actually be observed as the strong light halo around the beamblock in figure 3(b), that extends all the way through to the SPP crescents. In the IP the radiation background can easily lead to a perceived longer decay which is interpreted as a longer L_{SPP} . Since in the FP the scattered radiation and the SPP light are separated, more realistic and true values for the SPP-decay length can be determined using the FP profiles and fitting the Lorentzian peaks.

Finally, the real part of the SPP wave vector $(k_x)_r$ can be determined from the position of the maximum of the SPP signature in the FP. The positions of the crescents are obtained

from the centre values of the fitted Lorentzian peaks. Figure 3(b) yields $(k_x)_r = 8.3 \mu\text{m}^{-1}$, $8.6 \mu\text{m}^{-1}$, $8.7 \mu\text{m}^{-1}$ and $10.1 \mu\text{m}^{-1}$ for the SPP-wave vectors of the bulk gold, 30 nm, 55 nm hexaporous gold, and dealloyed gold, respectively.

Although a direct comparison with experimental data of the reflection measurements in Kretschmann configuration is not possible because reflection dips have not been recorded at the wavelength of 780 nm, the theoretically determined dispersion curves show a good agreement with both, the reflection data and the specific LRM measurements at 780 nm for the bulk and ordered hexaporous gold samples. Applying the effective medium formulas at a wavelength of 780 nm result in theoretical SPP-wave vectors of $8.2 \mu\text{m}^{-1}$, $8.4 \mu\text{m}^{-1}$, $8.4 \mu\text{m}^{-1}$ and $9.03 \mu\text{m}^{-1}$ for the of the bulk gold, 30 nm, 55 nm hexaporous gold, and dealloyed gold, respectively. These results demonstrate clearly how the structure of the nanoporous gold and the level of porosity influence the SPP dispersion and the material optical properties.

Comparing the two experimental methods, angular dependent reflection spectroscopy and LRM, the LRM showed several advantages. In LRM both, the real and imaginary part of the SPP wave vector can be determined very accurately using the FP images. The observed features are reasonably sharp and a comparison to the real image allows a quick check for reliability. However, LRM has been used only for one specific laser wavelength. Spectroscopic measurements would require other light or laser sources. This is the strength of the applied reflection spectroscopy in Kretschmann configuration which can be used to map the SPP-dispersion relation within the whole near IR and visible spectral region. Unfortunately, the dips are very wide for spectra taken at fixed angular positions which complicates the determination of the exact SPP-resonances especially for SPPs experiencing higher losses i.e. wider resonances. The extended width of the dips is caused by the nature of the measurement. Measuring the wavelength at a fixed angle means that one follows an inclined line similar like the light line through the dispersion diagram (see figure 4). This measuring line intersects the SPP dispersion curve under a small angle resulting in a long way through the ‘resonance valley’. The situation is different for the LRM which operates at a fixed frequency and basically cuts the dispersion curve along a horizontal line leading to a sharper, better defined resonance in the FP.

4. Summary

In conclusion different types of nanoporous gold films have been fabricated and studied with respect to tailor the plasmonic response of gold by introducing different levels of porosity. Reflection spectroscopy in Kretschmann configuration has revealed a substantial red shift of the SPP dispersion relation on the nanoporous gold with respect to its bulk counterpart when the porosity reaches levels of the order of 50%. These results have been found to be in good agreement with theoretical predictions based on effective medium models for the nanoporous films. Additional leakage radiation analysis has been used to determine SPP propagation lengths on the order of 4–5 μm for the nanoporous samples. The results demonstrate that a control of the metal permittivity and the connected surface plasmon dispersion relation is possible by introducing a nanoporosity. The observed SPPs therefore represent designer plasmons in the visible and near infrared spectral region. The price for this flexibility are increased scattering losses due to the surface roughness and electron surface scattering in small metallic veins in the material. However, applications where a substance has to be infiltrated into narrow channels within a metal to experience a strong plasmon field, e.g. SERS and sensing applications as well

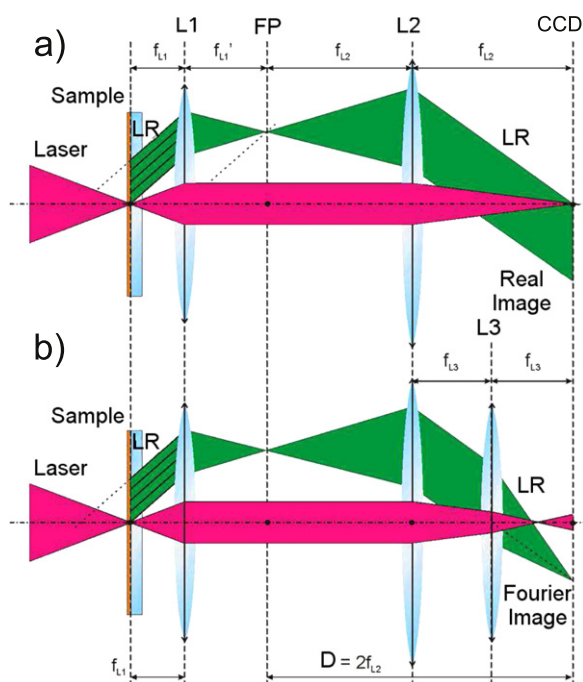


Figure A1. Leakage radiation microscopy setup (a) real plane imaging, (b) Fourier plane imaging.

as fluorescence enhancement processes, where the dispersion relation of the surface plasmon should be tuned to a specific wavelength, will benefit from this class of simple plasmonic metamaterials.

Acknowledgments

The authors thank the Fraunhofer Institute (IWMH), for FIB milling and the Federal Ministry for Education and Research (BMBF) for the financial support under project number FKZ:03Z2HN12, within the Centre for Innovation Competence SiLi-nano. The authors further acknowledge financial support of this work by the priority programmes SPP1391 ‘Ultrafast Nanooptics’ and SPP 1327 ‘Optically Generated Sub-100 nm Structures for Technical and Biomedical Applications’ of the Deutsche Forschungsgemeinschaft (DFG), the Volkswagen-Stiftung within the project ‘Nanostrukturierte Polymere für Anwendungen in der Optik / Nanostructured Polymers for Applications in Optics’, and the Collaborative Research Center / Transregio 123 ‘Planar Optronics Systems’ of the German Research Foundation (Deutsche Forschungsgemeinschaft, DFG). The authors further acknowledge support by the Center for Quantum Engineering and Space-Time Research (QUEST), and the Laboratory of Nano- and Quantum Engineering (LNQE) of the Leibniz University Hannover.

Appendix

LRM setup is shown in [A1](#). The magnified view of the intensity profile of Bulk gold is shown in [A2](#).

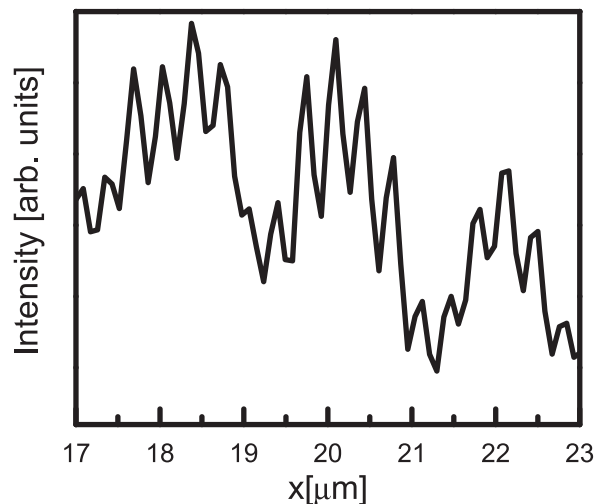


Figure A2. Magnified view of the intensity profile of Bulk gold from figure 3(a) revealing the long and short range oscillations $\Lambda_{l,s}$.

References

- [1] Ziolkowski R W 2004 Propagation in and scattering from a matched metamaterial having a zero index of refraction *Phys. Rev. E* **70** 046608
- [2] Alù A and Engheta N 2005 Achieving transparency with plasmonic and metamaterial coatings *Phys. Rev. E* **72** 016623
- [3] Khurgin J B and Boltasseva A 2012 Reflecting upon the losses in plasmonics and metamaterials *MRS Bull.* **37** 768–79
- [4] Naik G V, Shalaev V M and Boltasseva A 2013 Alternative plasmonic materials: beyond gold and silver *Adv. Mater.* **25** 3264–94
- [5] Maier S A 2007 *Plasmonics: Fundamentals and Applications* (Berlin: Springer)
- [6] Fujita T, Qian L H, Inoke K, Erlebacher J and Chen M W 2008 Three-dimensional morphology of nanoporous gold *App. Phys. Lett.* **92** 251902
- [7] Shi Z, Piredda G, Liapis A C, Nelson M A, Novotny L and Boyd R W 2009 Analytical investigation of modulation instability in a fiber Bragg grating *Opt. Lett.* **34** 3527–535
- [8] Dixon M C, Daniel T A, Hieda M, Smilgies D M, Chan M H W and Allara D 2007 Surface-plasmon polaritons on metal-dielectric nanocomposite films *J. Am. Chem. Soc.* **23** 2414–22
- [9] Kanungo J and Schilling J 2010 Preparation, structure, and optical properties of nanoporous gold thin films *App. Phys. Lett.* **97** 021903
- [10] Pendry J B, Martín-Moreno L and Garcia-Vidal F J 2004 Experimental determination of the principal dielectric functions in silver nanowire metamaterials *Science* **305** 847–8
- [11] Hibbins A P, Evans B R and Sambles J R 2005 Mimicking surface plasmons with structured surfaces *Science* **308** 670–2
- [12] Nesterov M L, Martin-Cano D, Fernandez-Dominguez A I, Moreno E, Martin-Moreno L and Garcia-Vidal F J 2010 Geometrically induced modification of the surface plasmons in the optical and telecom regimes *Opt. Lett.* **35** 423–25
- [13] Raether H 1988 *Surface Plasmons on Smooth and Rough Surfaces and on Gratings* vol 111 (Berlin: Springer)
- [14] Drezet A, Hohenau A, Stepanov A L, Ditlbacher H, Steinberger B, Galler N, Aussenegg F R, Leitner A and Krenn J R 2006 How to erase surface plasmon fringes *App. Phys. Lett.* **89** 091117

- [15] Drezet A, Hohenau A, Koller D, Stepanov A L, Ditlbacher H, Steinberger B, Aussenegg F R, Leitner A and Krenn J R 2008 Leakage radiation microscopy of surface plasmon polaritons *Mater. Sci. Eng. B* **149** 220–9
- [16] Hohenau A, Krenn J R, Drezet A, Mollet O, Huan S, Genet C, Stein B and Ebbesen T W 2011 Surface plasmon leakage radiation microscopy at the diffraction limit *Opt. Express* **19** 25749–62
- [17] Sardana N, Heyroth F and Schilling J 2012 Propagating surface plasmons on nanoporous gold *J. Opt. Soc. Am. B* **29** 1778–83
- [18] Seidel A, Reinhardt C, Holmgaard T, Cheng W, Rosenzweig T, Leosson K, Bozhevolnyi S I and Chichkov B N 2010 Demonstration of laser-fabricated dlspw at telecom wavelength *IEEE Photon. J.* **2** 652–8
- [19] Reinhardt C, Seidel A, Evlyukhin A B, Cheng W, Kiyani R and Chichkov B N 2010 Direct laser-writing of dielectric-loaded surface plasmon-polariton waveguides for the visible and near infrared *Appl. Phys. A* **100** 347–52
- [20] Kiyani R, Reinhardt C, Passinger S, Stepanov A L, Hohenau A, Krenn J R and Chichkov B N 2007 Rapid prototyping of optical components for surface plasmon polaritons *Opt. Express* **15** 4205–15
- [21] Reinhardt C, Seidel A, Evlyukhin A B, Cheng W and Chichkov B N 2009 Mode-selective excitation of laser-written dielectric-loaded surface plasmon polariton waveguides *J. Opt. Soc. Am. B* **26** 55–60
- [22] Reinhardt C, Evlyukhin A B, Cheng W, Birr T, Markov A, Ung B, Skorobogatiy M and Chichkov B N 2013 Bandgap-confined large-mode waveguides for surface plasmon-polaritons *J. Opt. Soc. Am. B* **30** 2898–905
- [23] Paz V F, Emons M, Obata K, Ovsianikov A, Peterhaensel S, Frenner K, Reinhardt C, Chichkov B N, Morgner U and Osten W 2012 Development of functional sub-100 nm structures with 3d two-photon polymerization technique and optical methods for characterization *J. Laser Appl.* **24** 042004
- [24] Bruggeman D A G 1935 Berechnung verschiedener physikalischer konstanten von heterogenen substanzen *Ann. Phys., Lpz.* **416** 636–64
- [25] Garnett J C M 1904 Colours in metal glasses and in metallic films *Phil. Trans. R. Soc. London* **203** 385–420